IEEE Access
Multidisciplinary | Rapid Review | Open Access Journal

SPECIAL SECTION ON RECENT ADVANCES IN VIDEO CODING AND SECURITY

Received May 14, 2019, accepted June 8, 2019, date of publication June 26, 2019, date of current version July 17, 2019.

Digital Object Identifier 10.1109/ACCESS.2019.2925087

Automatic Gauge Detection via Geometric Fitting for Safety Inspection

BEICHEN LI[1], JINGYU YANG[1], (Senior Member, IEEE), XINYANG ZENG[1], HUANJING YUE[1], AND WEI XIANG[2], (Senior Member, IEEE)

[1]School of Electrical and Information Engineering, Tianjin University, Tianjin 300072, China
[2]College of Science and Engineering, James Cook University, Townsville, QLD 4810, Australia

Corresponding authors: Huanjing Yue (dayueer@tju.edu.cn) and Wei Xiang (wei.xiang@jcu.edu.au)

This work was supported by the National Natural Science Foundation of China under Grant 61771339, Grant 61571322, and Grant 61520106002.

ABSTRACT For safety considerations in electrical substations, the inspection robots are recently deployed to monitor important devices and instruments with the presence of skilled technicians in the high-voltage environments. The captured images are transmitted to a data station and are usually analyzed manually. Toward automatic analysis, a common task is to detect gauges from captured images. This paper proposes a gauge detection algorithm based on the methodology of geometric fitting. We first use the Sobel filters to extract edges which usually contain the shapes of gauges. Then, we propose to use line fitting under the framework of random sample consensus (RANSAC) to remove straight lines that do not belong to gauges. Finally, the RANSAC ellipse fitting is proposed to find most fitted ellipse from the remaining edge points. The experimental results on a real-world dataset captured by the GuoZi Robotics demonstrate that our algorithm provides more accurate gauge detection results than several existing methods.

INDEX TERMS Computer vision, object detection, pressure gauges.

I. INTRODUCTION

Transformer substations step down high-voltage electricity from power lines into low-voltage electricity for urban usage. Such substations involve many special devices, whose operating states are monitored by various instruments. Being exposed in complex temperature-humidity-radiation conditions, these instruments also need manual inspection and maintenance. However, the intense radiation impose considerable risks to human health. Thus, it is desirable to use robots to inspect instruments such gauges. To this end, inspection robots are equipped with various sensors such as visible-light camera, infrared cameras, or/and Lidar. A typical robot inspection routine includes the following steps: 1) stop at a pre-defined location with inspection tasks; 2) adjust the pose of cameras and capture pictures of the targets; 3) repeat the previous two steps until the robot travels through the predefined path. Captured images are sent back to a monitoring center via wireless channels. The captured images are analyzed in the monitor center, e.g., detecting potential defects of the instruments and reading out the gauge values. To achieve this, the first step is to detect gauges from the captured images. The most straightforward way is to use template matching with SIFT [1] or SURF [2] features. However, this would require a pre-requisite dataset for the detected gauges, and somehow lack generalization capability as the substations may change the gauges, and different substations may also use different gauges. The alternative approach is to train a prevalent neural network which can categorize these objects automatically. But unfortunately, training a deep neural network with promising generalization would require considerable amount of data, which is difficult to collect. We note that the shapes of gauges in captured images are circles or ellipse as shown in Fig. 1. As the captured image usually do not contain other objects, this observation motivates us to detect gauges by fitting geometrical shapes, which is robust to appearance change of various gauges.

FIGURE 1. Comparison of detected shapes of gauges with different methods. From left to right: the input gauge images, CHT method and our method.

The associate editor coordinating the review of this manuscript and approving it for publication was Zhaoqing Pan.

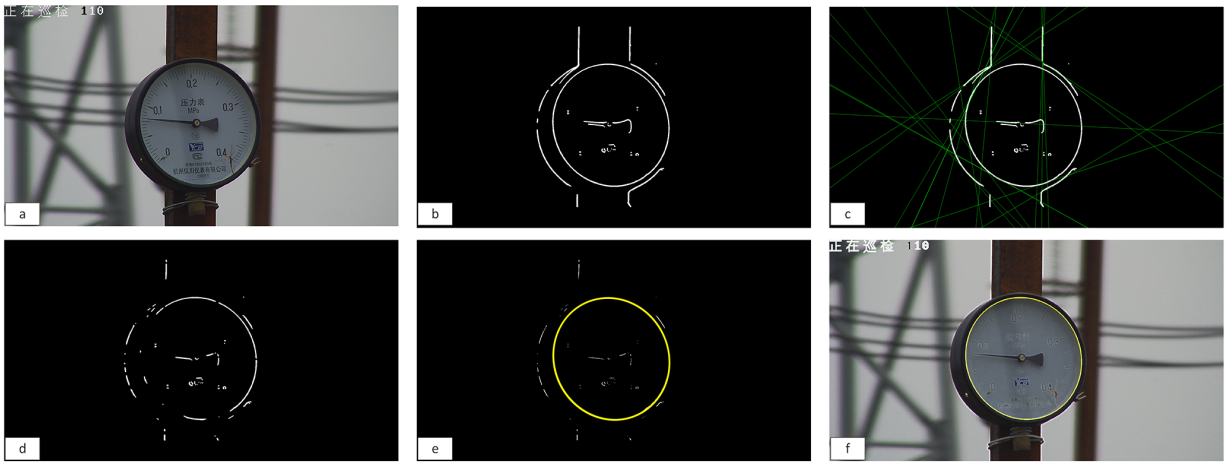

FIGURE 2. Steps of our gauge detection method: a) the input gauge image, b) result of edge detection, c) result of the line fitting, d) result of line removal, e) result of ellipse fitting and d) the superposition of the result of ellipse fitting and the original input gauge image.

Based on the analysis above, we propose a gauge detection method based on the geometric fitting approach. Concretely, we first utilize a set of Sobel filters to detect edges. The lines in the edge maps (corresponding to the pillar holding the gauge) are removed via line fitting with random sample consensus (RANSAC) [3]. Finally, RANSAC ellipse fitting is proposed to detect the shapes of gauges. The proposed approach does not need template and is accurate and fast. Experimental results show that the proposed algorithm is able to reliably detect gauges from real images captured from substations, outperforming several existing methods.

II. RELATED WORK

The most related work to our work is circle detection. For circle detection, the most common strategy is applying Circular Hough Transform [4] (CHT). This strategy first applies edge detector, such as Canny edge detection, to detect the edges, and then utilize the edge information to predict the location of the circle. This strategy costs a large storage space. The computational complexity is also high and the processing speed is low. In addition, the detection accuracy is poor, especially under noisy conditions [5]. It is difficult for CHT to process images with high resolution in real time. To solve this problem, many approaches are proposed by researchers. For example, the Probabilistic Hough transform [6], the randomized Hough transform (RHT) [7] and the fuzzy Hough transform [8]. Lu and Tan [9] proposed an Iterative Randomized Hough Transformation (IRHT) and achieved promising results on noisy and complex images. The algorithm iteratively utilizes RHT to the region determined from the latest estimation of circle parameters.

Besides Hough transform, there are some optimization based methods for circle detection. Ayalaamirez *et al.* [10] presented a circle detector based on a genetic algorithm, but it usually cannot handle imperfect circles. Dasgupta *et al.* [11] proposed an automatic circle detector using the Bacterial Foraging Algorithm (BFAOA) as an optimization method. The two methods demand the algorithm to repeatedly perform in order to detect multiple circles. The work in [12] utilized the Clonal Selection Algorithm (CSA) to detect multiple-circles, which assumes that the detection process is a multi-modal optimization problem. Cuevas *et al.* [13] proposed a fast circle detection method utilizes Learning Automana (LA), which has lower computing complexity. The LA method searches within the probability space rather than exploring the parameter space as commonly done by other optimization techniques.

Different from them, we propose a very simple but effective gauge detection method. We first extract contours of gauges by the gradient information, then utilize RANSAC fitting to remove unnecessary lines. Then we propose an ellipse fitting algorithm to fit the shapes of gauges.

III. METHOD

Our proposed gauge detection method consists of three steps, i.e. edge extraction, line removal, and ellipse fitting. In the following, we give a detailed description of the three steps, and typical results of these steps are shown in Fig. 2.

A. EDGE DETECTION

To successfully detect shapes, we first detect the edges from the input image with Sobel kernels. Since the captured images may be contaminated by noise, we first utilize a $K \times K$ median filter to suppress the noise. The kernels used for edge detection are denoted by S_x and S_y, where subscripts x and y denotes the horizontal and vertical directions of kernels, respectively. The two kernels are defined as follows.

$$S_x = \begin{bmatrix} -1 & 0 & 1 \\ -2 & 0 & 2 \\ -1 & 0 & 1 \end{bmatrix}, \quad S_y = \begin{bmatrix} -1 & -2 & -1 \\ 0 & 0 & 0 \\ 1 & 2 & 1 \end{bmatrix}. \quad (1)$$

Let X be the input image after the median filtering. Then, the filtering by the Sobel kernels generate two high-passed images:

$$\begin{aligned} X_{hx} &= S_x * X, \\ X_{hy} &= S_y * X, \end{aligned} \quad (2)$$

where '$*$' denotes the convolution operator. Then the edge map, denoted by E_1, is obtained by the union of binarized edge maps from X_{hx} and X_{hy}:

$$E_1 = \mathcal{B}_\tau(|X_{hx}|) \cup \mathcal{B}_\tau(|X_{hx}|), \tag{3}$$

where '$\cup$' denotes the union of two sets. The binarization operator $\mathcal{B}$ with the threshold τ is defined as

$$\mathcal{B}_\tau(x) = \begin{cases} 1, & x \geq \tau, \\ 0, & x < \tau. \end{cases} \tag{4}$$

The threshold for binarization is set as $\tau = 255/3$ in our implementation.

X_{hx} and X_{hy} extract vertical and horizontal edge information, respectively. Fusing the two sets of complementary edge information, edge map E_1 contains most prominent edges in the image for the subsequent shape fitting. Fig. 2 (b) shows the fused edge maps.

B. LINE REMOVAL

However, as shown in Fig. 2 (b), we observe that there are some straight lines that do not belong to the shape of the targeted gauges. The straight line would interfere the estimate of gauge shapes, and therefore should be removed. We propose to use the RANSAC [3] approach to fit the straight lines. The line model is defined as

$$y = kx + b, \tag{5}$$

where $\mathbb{p} \triangleq (x, y)$ denotes the image coordinate, k and b are the slop and intersect, respectively. For compact presentation, denote a point by $\mathbb{p} \triangleq (x, y)$, and a line by $\ell \triangleq \{y = kx + b, x \in \mathbb{R}\}$. Given a pair of points $(\mathbb{p}_1, \mathbb{p}_2)$, the line is uniquely determined by

$$\begin{aligned} k &= \frac{y_2 - y_1}{x_2 - x_1}, \\ b &= y_1 - kx_1. \end{aligned} \tag{6}$$

Note that special cases for $x_1 = x_2$ are detected and treated separately to avoid division by zero. To fit lines in the image, we first generate K_l line proposals $\left\{\ell^k, k = 1, \ldots, K_l\right\}$ by K_l randomly drawing point pairs $\left\{(\mathbb{p}_1^k, \mathbb{p}_2^k), k = 1, \ldots, K_l\right\}$ from the extracted edge map E_1. As long as K_l is large enough, there would be some proposals hitting the lines to be detected. To select the fitted ones, we count the number of inlier points for each line proposal, and select the ones with largest inliers. A point $\mathbb{p}$ is considered as an inlier of a line ℓ if $\mathbb{p}$ is close by ℓ. Concretely, the distance from $\mathbb{p}$ to ℓ is defined as $\mathcal{D}(\mathbb{p}, \ell) \triangleq |y - kx - b|/\sqrt{1 + k^2}$. The inlier points of line ℓ^k is defined as $\mathbb{I}^k \triangleq \{\mathbb{p} | \mathcal{D}(\mathbb{p}, \ell^k) < \epsilon, \mathbb{p} \in \mathbb{P}_1\}$. Then, the proposals with top 20% largest number of inliers are chosen as fitted lines. The inlier points associated with the fitted lines are removed from $\mathbb{P}_1$ to reduce the interference in the subsequent ellipse fitting. Denote by $\mathbb{P}_2$ the point set after removing line inliers. Then, $\mathbb{P}_2$ is determined as

$$\mathbb{P}_2 = \mathbb{P}_1 \setminus \cup_{k=1}^{K_l} \mathbb{I}^k. \tag{7}$$

The associated edge map E_2 after line removal from E_1 is obtained for subsequent geometrical fitting. Fig. 2 (d) shows that lines are effectively removed through the RANSAC line fitting approach.

C. ELLIPSE FITTING

1) ELLIPSE ESTIMATION

To estimate the latent ellipse from the edge map E_2, we propose using RANSAC to perform ellipse fitting from the associated point set $\mathbb{P}_2$. We start by establishing a model for estimating the coefficients of Conic Equation (CE) [14] using a set of points $\{\mathbb{p}_1, \mathbb{p}_2, \ldots, \mathbb{p}_N, N \geq 5\}$. The conic equation model is defined as

$$ax^2 + bxy + cy^2 + dx + ey + f = 0, \tag{8}$$

where a, b, c, d, e, f are CE coefficients. For simplicity, we normalize f as 1, and Eq. (8) is written as

$$\tilde{a}x^2 + \tilde{b}xy + \tilde{c}y^2 + \tilde{d}x + \tilde{e}y + 1 = 0. \tag{9}$$

We define $\boldsymbol{t} = [\tilde{a}, \tilde{b}, \tilde{c}, \tilde{d}, \tilde{e}]^\top$ as the vector of parameters to be estimated, $\boldsymbol{x} = [x_1, x_2, \ldots, x_N]^\top$, $\boldsymbol{y} = [y_1, y_2, \ldots, y_N]^\top$, $\mathbf{1} = [1, 1, \ldots, 1]^\top \in \mathbb{R}^{N \times 1}$, and $\boldsymbol{X} = [\boldsymbol{x}^2, \boldsymbol{x} \cdot \boldsymbol{y}, \boldsymbol{y}^2, \boldsymbol{x}, \boldsymbol{y}] \in \mathbb{R}^{N \times 5}$, where "$\cdot$" denotes element-wise multiplication. Based on the least squares method, CE parameters are obtained by minimized the following cost function:

$$Cost(\boldsymbol{t}) = ||\boldsymbol{X}\boldsymbol{t} + \mathbf{1}||^2. \tag{10}$$

Estimator vector $\boldsymbol{t}^* = [a^*, b^*, c^*, d^*, e^*]^\top$ is yielded by taking the derivation of the cost function with respect to $\boldsymbol{t}$:

$$\boldsymbol{t}^* = -(\boldsymbol{X}^\top \boldsymbol{X})^{-1} \boldsymbol{X}^\top \mathbf{1}. \tag{11}$$

If $\boldsymbol{t}^*$ satisfies $a^* c^* > 0$ (we hold a^* positive), Eq. (9) is denoted as a General Ellipse Equation (GEE). Note that an ellipse has a tilt when the cross term xy has a non-zero coefficient. However, a tilted ellipse is difficult to find its foci. For the sake of simplicity, a tilted ellipse is transformed into a non-tilted one. General Non-tilted Ellipse Equation (GNEE) is defined as

$$a_g x'^2 + c_g y'^2 + d_g x' + e_g y' + 1 = 0. \tag{12}$$

We remove the tilt with the following substitution:

$$\begin{cases} x = x' \cos\phi + y' \sin\phi, \\ y = -x' \sin\phi + y' \cos\phi. \end{cases} \tag{13}$$

According to Eq. (9) and Eq. (13), ϕ is determined as:

$$\phi = \frac{1}{2} \arctan\left(\frac{b^*}{c^* - a^*}\right). \tag{14}$$

Therefore GNEE coefficients a_g, c_g, d_g, e_g in Eq. (12) are determined as:

$$\begin{cases} a_g = a^* \cos^2\phi - b^* \cos\phi \sin\phi + c^* \sin^2\phi, \\ c_g = a^* \sin^2\phi + b^* \cos\phi \sin\phi + c^* \cos^2\phi, \\ d_g = d^* \cos\phi - e^* \sin\phi, \\ e_g = d^* \sin\phi + e^* \cos\phi. \end{cases} \tag{15}$$

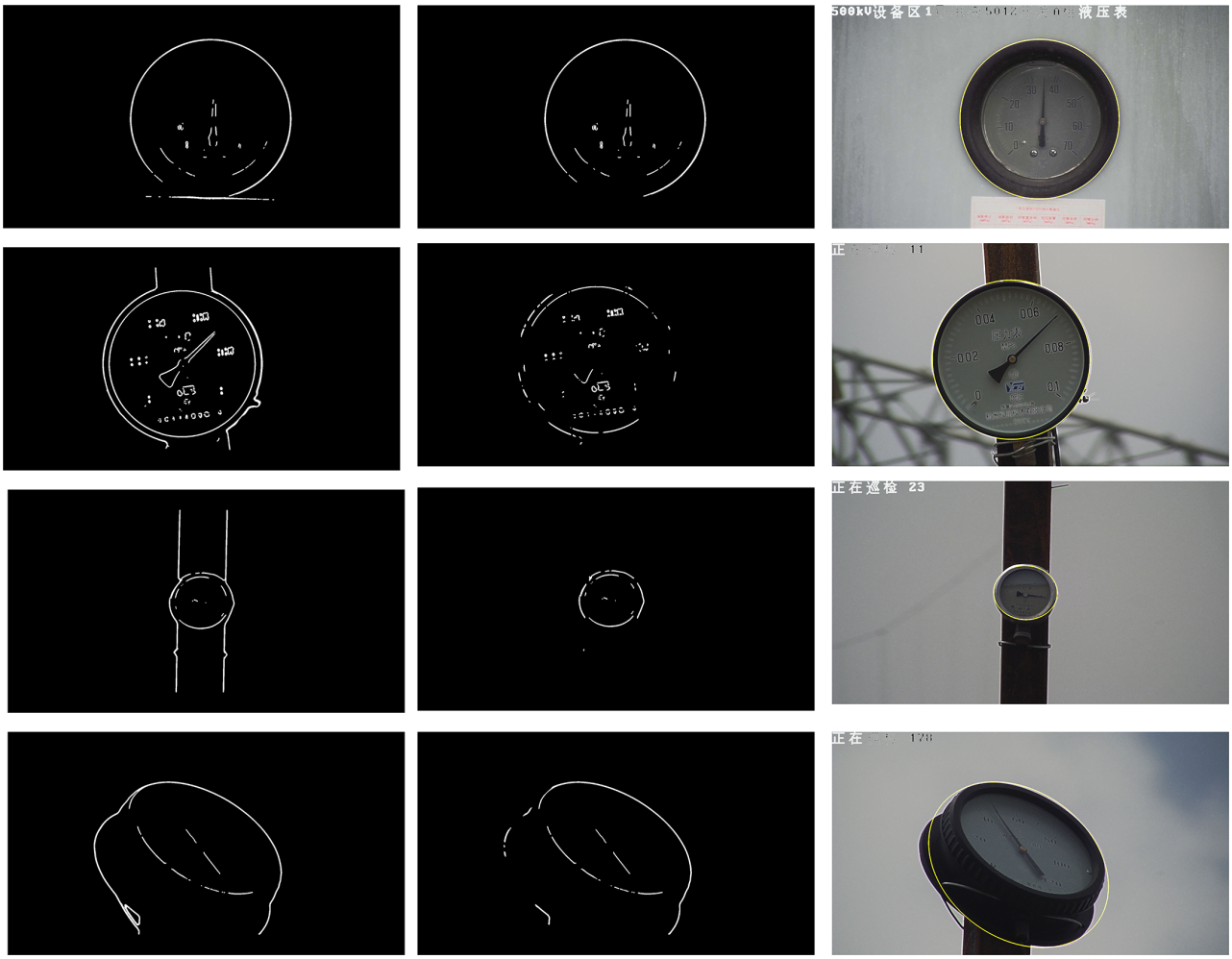

FIGURE 3. Intermediate results generated by our methods. From left to right: the arc map, line removal result and the superposition of the detected ellipse and the original input.

We define the Standard Non-tilted Ellipse Equation (SNEE) as

$$\frac{(x'-x_0)^2}{a_s}+\frac{(y'-y_0)^2}{b_s}=1, \tag{16}$$

where (x_0, y_0) is the center of the ellipse, a_s, b_s are the ellipse "radiuses". According to Eq. (12) and Eq. (16), we obtain SNEE parameters in terms of the GNEE ones:

$$\begin{cases} x_0 = -d_g/(2a_g), \\ y_0 = -e_g/(2c_g), \\ a_s = \sqrt{|K/a_g|}, \\ b_s = \sqrt{|K/c_g|}, \end{cases} \tag{17}$$

where K is defined as

$$K = -1 + d_g^2/4a_g + e_g^2/4c_g. \tag{18}$$

The foci $(\mathbb{f}_1, \mathbb{f}_2)$ of the ellipse are determined as follows:

(i) if $a_s \geq b_s$:

$$\mathbb{f}_1 = \boldsymbol{r}^\top \left[x_0 + \sqrt{a_s^2 - b_s^2}, y_0\right]^\top,$$

$$\mathbb{f}_2 = \boldsymbol{r}^\top \left[x_0 - \sqrt{a_s^2 - b_s^2}, y_0\right]^\top, \tag{19}$$

(ii) if $a_s < b_s$:

$$\mathbb{f}_1 = \boldsymbol{r}^\top \left[x_0, y_0 + \sqrt{b_s^2 - a_s^2}\right],$$

$$\mathbb{f}_2 = \boldsymbol{r}^\top \left[x_0, y_0 - \sqrt{b_s^2 - a_s^2}\right], \tag{20}$$

where

$$\boldsymbol{r} = [\cos\phi \sin\phi, -\sin\phi \cos\phi]^\top. \tag{21}$$

Without loss of generality, we assume $a_s > b_s$. Based on the property of an ellipse $\mathcal{E}$, the distances from a point $\mathbb{p} \in \mathcal{E}$ to $\mathbb{F}_1$ and $\mathbb{F}_2$ adds up to a constant, which equals to the length of long axis:

$$\|\mathbb{p}\mathbb{f}_1\| + \|\mathbb{p}\mathbb{f}_2\| = 2a_s, \tag{22}$$

where $\|\cdot\|$ denotes the distance between two points.

TABLE 1. Comparison of gauge detection results.

Ours	94.43%	86.60%	89.40%
CHT	79.43%	68.83%	72.78%
SQDIFF	37.99%	67.56%	45.86%
CCORR	7.74%	18.56%	10.01%
CCOEFF	44.51%	90.68%	55.29%
SQDIFF_NORM	25.31%	45.88%	30.91%
CCORR_NORM	17.05%	27.54%	20.15%
CCOEFF_NORM	43.52%	87.08%	53.69%

2) RANSAC ELLIPSE FITTING

To fit an ellipse from edge map E_2, we first generate K_e ellipse proposals $\left\{\mathcal{E}^k(\mathbb{f}_1^k, \mathbb{f}_2^k, a_s^k, b_s^k), k = 1, \ldots, K_e\right\}$ by K_e randomly point sets $\left\{(\mathbb{p}_1^k, \ldots, \mathbb{p}_N^k), k = 1, \ldots, K_e, N = 5\right\}$ from the extracted edge map E_2. Some proposals hitting the ellipses would be detected as long as K_e is large enough. To select the fitted ellipse, we count the number of inlier points for each ellipse proposal, and select the ellipses with top 5 largest member of inliers for refinement. A point $\mathbb{p}$ is considered as an inlier of an ellipse $\mathcal{E}$ if $\mathbb{p}$ is close by $\mathcal{E}$. According to Eq. (22), the inlier points of ellipse $\mathcal{E}^k$ is defined as $\mathbb{E}^k \triangleq \left\{\mathbb{p} \,\middle|\, \left|\|\mathbb{p}\mathbb{f}_1^k\| + \|\mathbb{p}\mathbb{f}_2^k\| - 2a_s^k\right| < \epsilon_2, \mathbb{p} \in \mathbb{P}_2\right\}$. The ellipse proposals with top five largest number of inliers are selected, denoted by $\{\bar{\mathcal{E}}^k\}_{k=1}^5$. The associated inlier points are denoted by $\{\bar{\mathbb{E}}^k\}_{k=1}^5$, for the selected ellipses respectively. Then, the final ellipse is estimated from the collected inlier points $\cup_{k=1}^5 \bar{\mathbb{E}}^k$. Fig. 2 (e) shows that ellipses are detected through our ellipse fitting approach.

IV. EXPERIMENTAL RESULTS

In this section, we first present our intermediate results for edge extraction, line removal, and ellipse fitting. Then, we compare the proposed method with various methods based on Hough transform and template matching.

A. INTERMEDIATE RESULTS

To further demonstrate the effectiveness of the proposed three-step based gauge detection method, we present the intermediate results generated by our method for four images, as shown in Fig.3. The four images represent the typical cases where the pressure gauges are captured. It can be observed that the generated edge map contains candidate pixels of the gauge shape. The line removal algorithm works well in removing straight lines, and the ellipse fitting algorithm is good at recovering the most possible ellipse from the line removal result. The detected ellipse fits well with the pressure gauge, even if the pressure gauge is mixed with complex background.

B. COMPARISON WITH OTHER METHODS

Our method is evaluated on a real-world dataset provided by GuoZi Robotics, which contains 118 images of pressure gauges.

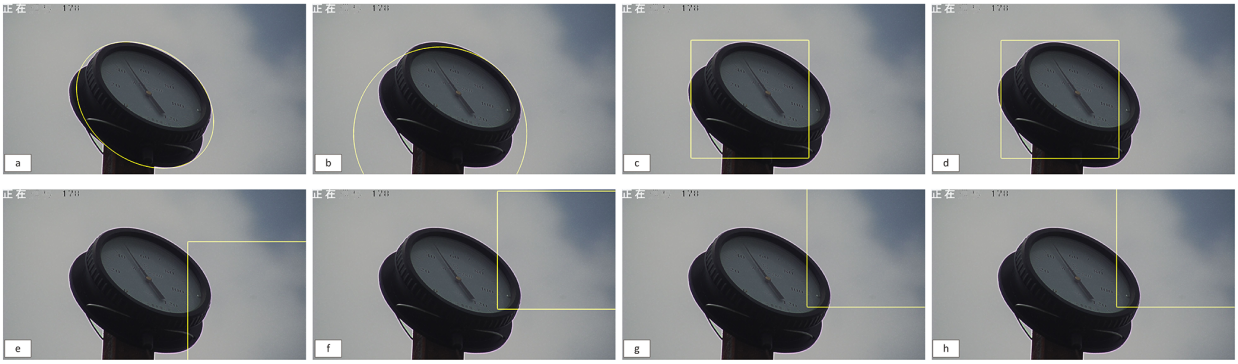

FIGURE 4. Visual comparison results. a) Ours, b) CHT, c) CCOEFF, d) CCOEFF_NORM, e) CCORR, f) CCORR_NORM, g) SQDIFF and h) SQDIFF_NORM.

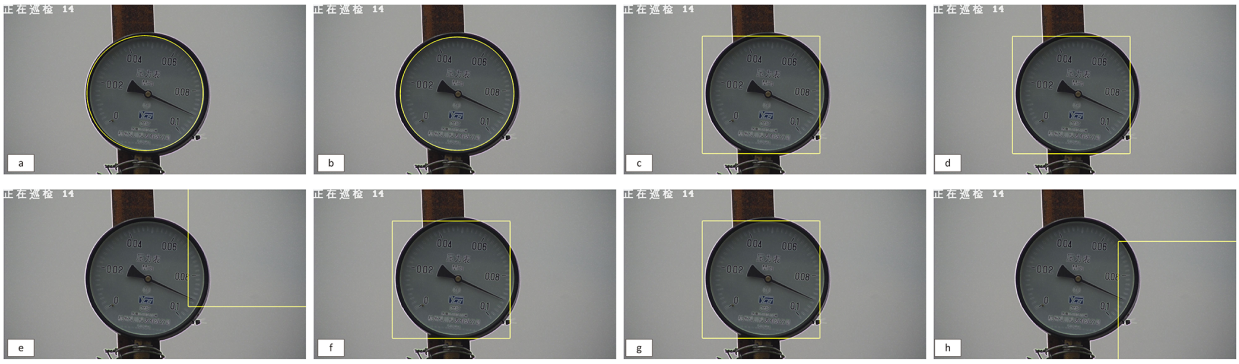

FIGURE 5. Visual comparison results. a) Ours, b) CHT, c) CCOEFF, d) CCOEFF_NORM, e) CCORR, f) CCORR_NORM, g) SQDIFF and h) SQDIFF_NORM.

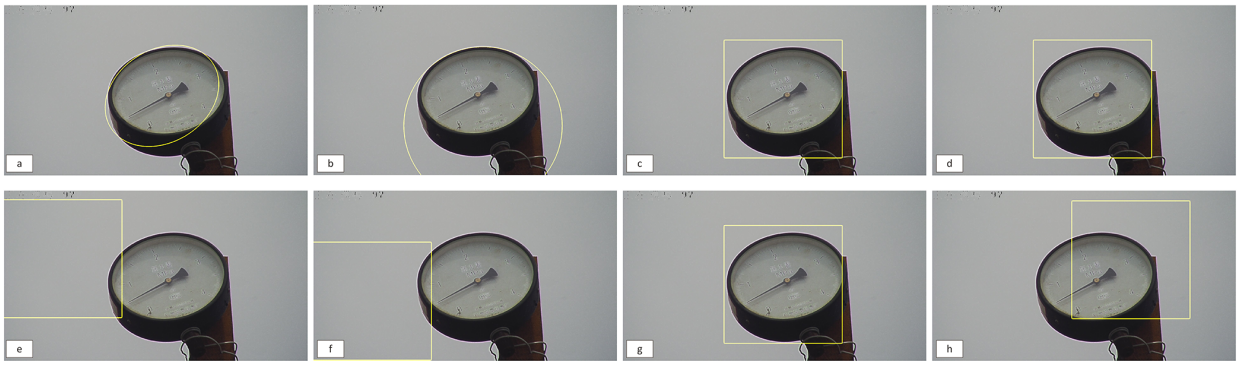

FIGURE 6. Visual comparison results. a) Ours, b) CHT, c) CCOEFF, d) CCOEFF_NORM, e) CCORR, f) CCORR_NORM, g) SQDIFF and h) SQDIFF_NORM.

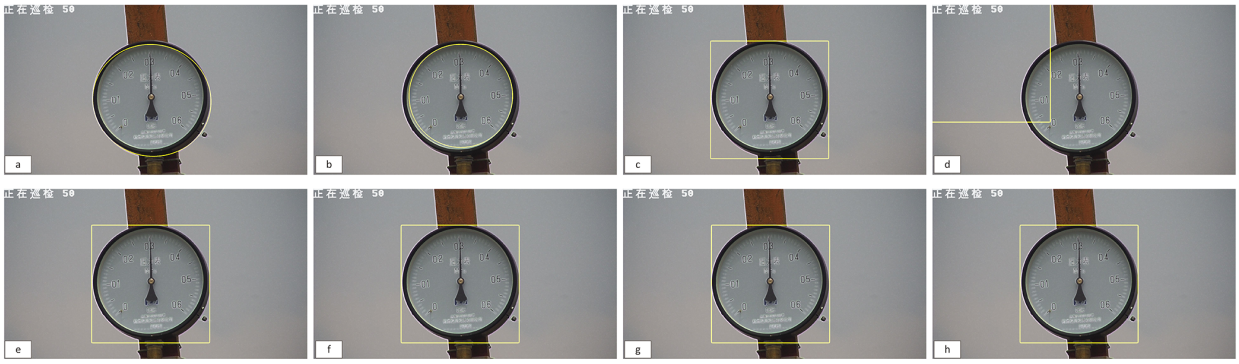

FIGURE 7. Visual comparison results. a) Ours, b) CHT, c) CCOEFF, d) CCOEFF_NORM, e) CCORR, f) CCORR_NORM, g) SQDIFF and h) SQDIFF_NORM.

In this subsection, we compare the proposed gauge detection method with several existing methods and their variants: the circle detection based on Hough transform (CHT), and detection methods based template matching using different cost functions, i.e., sum of square difference (SQDIFF), correlation (CCORR), correlation coefficient (CCOEFF), and their normalized versions.

The performance of the detection is evaluated both subjectively and objectively. For objective evaluation, we manually label the gauges for all the images in our dataset to serve as the ground truth. Then, for the detection results, we calculate the Precision, Recall, and F-score to evaluate the detection performance. Table 1 presents the comparison results. Our method achieves the best results compared with other methods.

For subjective evaluation, we present the comparison results for all the above methods in Fig. 4∼7. It can be observed that our method obtains the most appropriate detection results for gauges captured under looking-straight or looking-up/down viewpoints. Meanwhile, the CDHT method works well for the gauges captured under looking-straight viewpoints and cannot work well when the gauges are captured under looking-down viewpoints, as shown in Fig. 4 and 6. This further demonstrates the generality of the proposed method in dealing with different kinds of gauge images.

V. CONCLUSION

This paper proposes a novel and quite effective gauge detection algorithm. We first detect edges from the input gauge images utilize Sobel filter. Then we remove the straight lines which do not belong to the gauges using a RANSAC based line fitting algorithm. We propose an ellipse fitting algorithm to find the most fitted ellipse to the targeted gauge. Experiment results demonstrate that the proposed algorithm outperforms the classical CHT algorithm and its variants in both objective and subjective measurements.

REFERENCES

[1] D. G. Lowe, "Distinctive image features from scale-invariant keypoints," *Int. J. Comput. Vis.*, vol. 60, no. 2, pp. 91–110, 2004.

[2] H. Bay, T. Tuytelaars, and L. V. Gool, "SURF: Speeded up robust features," in *Proc. Eur. Conf. Comput. Vis.* Berlin, Germany: Springer, 2006, pp. 404–417.

[3] M. A. Fischler and R. Bolles, "Random sample consensus: A paradigm for model fitting with applications to image analysis and automated cartography," *Commun. ACM*, vol. 24, no. 6, pp. 381–395, 1981.

[4] H. Muammar and M. Nixon, "Approaches to extending the Hough transform," in *Proc. Int. Conf. Acoust., Speech, Signal Process.*, May 1989, pp. 1556–1559.

[5] T. J. Atherton and D. J. Kerbyson, "Using phase to represent radius in the coherent circle Hough transform," in *Proc. IEE Colloq. Hough Transforms*, London, U.K., May 1993, pp. 51–54.

[6] D. Shaked, O. Yaron, and N. Kiryati, "Deriving stopping rules for the probabilistic Hough transform by sequential analysis," *Comput. Vis. Image Understand.*, vol. 63, no. 3, pp. 512–526, 1996.

[7] L. Xu, E. Oja, and P. Kultanen, "A new curve detection method: Randomized Hough transform (RHT)," *Pattern Recognit. Lett.*, vol. 11, no. 5, pp. 331–338, 1990.
[8] J. H. Han, L. T. Koczy, and T. Poston, "Fuzzy Hough transform," in *Proc. 2nd IEEE Int. Conf. Fuzzy Syst.*, Mar./Apr. 1993, pp. 803–808.
[9] W. Lu and J. Tan, "Detection of incomplete ellipse in images with strong noise by iterative randomized Hough transform (IRHT)," *Pattern Recognit.*, vol. 41, no. 4, pp. 1268–1279, 2008.
[10] V. Ayala-Ramirez, C. H. Garcia-Capulin, A. Perez-Garcia, and R. E. Sanchez-Yanez, "Circle detection on images using genetic algorithms," *Pattern Recognit. Lett.*, vol. 27, no. 6, pp. 652–657, 2006.
[11] S. Dasgupta, S. Das, A. Biswas, and A. Abraham, "Automatic circle detection on digital images with an adaptive bacterial foraging algorithm," *Soft Comput.*, vol. 14, no. 11, pp. 1151–1164, 2010.
[12] E. Cuevas, V. Osuna-Enciso, F. Wario, and D. Zaldívar, and M. Pérez-Cisneros, "Automatic multiple circle detection based on artificial immune systems," *Expert Syst. Appl.*, vol. 39, no. 1, pp. 713–722, 2012.
[13] E. Cuevas, V. Osuna-Enciso, F. Wario, and D. Zaldivar, and M. Pérez-Cisneros, "Fast algorithm for multiple-circle detection on images using learning automata," *IET Image Process.*, vol. 6, no. 8, pp. 1124–1135, 2012.
[14] A. Fitzgibbon, M. Pilu, and R. B. Fisher, "Direct least squares fitting of ellipses," in *Proc. 13th Int. Conf. Pattern Recognit.*, Vienna, Austria, Aug. 1996, pp. 253–257.

BEICHEN LI received the B.E. degree from the University of Electronic Science and Technology of China, Chengdu, China, in 2010, and the M.S. degree from the Stevens Institute of Technology, Hoboken, USA, in 2016. He is currently pursuing the Ph.D. degree with Tianjin University in the field of deep learning for computer vision and the Internet of Things. He was a Research Assistant with the Maritime Security Center, SIT, from 2014 to 2015. He worked for several companies, including Good Technology and Kingsoft Cloud, and his working experiences include quality assurance, software development, cloud service, data analysis, and big data processing.

JINGYU YANG (M'10–SM'17) received the B.E. degree from the Beijing University of Posts and Telecommunications, Beijing, China, in 2003, and the Ph.D. degree (Hons.) from Tsinghua University, Beijing, in 2009. He was with Microsoft Research Asia (MSRA), in 2011, within the MSRA's Young Scholar Supporting Program, and the Signal Processing Laboratory, EPFL, Lausanne, Switzerland, in 2012, and from 2014 to 2015. He has been a Faculty Member with Tianjin University, China, since 2009, where he is currently a Professor with the School of Electrical and Information Engineering. He has authored or coauthored over 80 high quality research papers, including dozens of IEEE Transactions and top conference papers. His research interests include image/video processing, 3D imaging, and computer vision. As a coauthor, he got the best 10% paper award in IEEE VCIP 2016 and the Platinum Best Paper award in IEEE ICME 2017. He served as the Special Session Chair in VCIP 2016 and the Area Chair in ICIP 2017. He was selected into the program for New Century Excellent Talents in University (NCET) from the Ministry of Education, China, in 2011, the Reserved Peiyang Scholar Program of Tianjin University, in 2014, and the Tianjin Municipal Innovation Talent Promotion Program, in 2015.

XINYANG ZENG is currently pursuing the B.E. degree with the School of Electrical and Information Engineering, Tianjin University, Tianjin, China. His research interest includes mainly in image processing.

HUANJING YUE received the B.S. and Ph.D. degrees from Tianjin University, Tianjin, China, in 2010 and 2015, respectively. She was an Intern with Microsoft Research Asia, from 2011 to 2012, and from 2013 to 2015. She visited the Video Processing Laboratory, University of California at San Diego, from 2016 to 2017. She is currently an Associate Professor with the School of Electrical and Information Engineering, Tianjin University. Her current research interests include image processing and computer vision. She received the Microsoft Research Asia Fellowship Honor, in 2013, and was selected into the Elite Scholar Program of Tianjin University, in 2017.

WEI XIANG (S'00–M'04–SM'10) received the B.Eng. degree in electronic engineering and the M.Eng. degree in electronic engineering from the University of Electronic Science and Technology of China, Chengdu, China, in 1997 and 2000, respectively, and the Ph.D. degree in telecommunications engineering from the University of South Australia, Adelaide, Australia, in 2004.

In 2004 and 2015, he was with the School of Mechanical and Electrical Engineering, University of Southern Queensland, Toowoomba, Australia. He is currently the Founding Professor and the Head of Discipline of Internet of Things Engineering, James Cook University, Cairns, Australia. Due to his instrumental leadership in establishing Australia's first accredited Internet of Things Engineering degree program, he was selected into Pearcy Foundation's Hall of Fame, in 2018. He has published over 250 peer-reviewed papers including three academic books and 130 journal articles. His research interests include the broad areas of communications and information theory, particularly the Internet of Things, and coding and signal processing for multimedia communications systems.

Dr. Xiang is an elected Fellow of the IET in UK and Engineers Australia. He received the TNQ Innovation Award, in 2016, and the Pearcey Entrepreneurship Award, in 2017, and the Engineers Australia Cairns Engineer of the Year, in 2017. He was a co-recipient of four Best Paper Awards at WiSATS'2019, WCSP'2015, IEEE WCNC'2011, and ICWMC'2009. He has been awarded several prestigious fellowship titles. He was named a Queensland International Fellow, from 2010 to 2011, by the Queensland Government of Australia, an Endeavour Research Fellow, from 2012 to 2013, by the Commonwealth Government of Australia, a Smart Futures Fellow, from 2012 to 2015, by the Queensland Government of Australia, and a JSPS Invitational Fellow jointly by the Australian Academy of Science and Japanese Society for Promotion of Science, from 2014 to 2015. He has severed in a large number of international conferences in the capacity of the General Co-Chair, the TPC Co-Chair, and the Symposium Chair. He is the Vice Chair of the IEEE Northern Australia Section. He was an Editor for the IEEE Communications Letters, from 2015 to 2017. He is an Associate Editor for Springer's *Telecommunications Systems*.